Review of Scientific Instruments ARTICLE pubs.aip.org/aip/rsi

Measurements of variable capacitance using single port radio frequency reflectometry

Cite as: Rev. Sci. Instrum. 94, 084703 (2023); doi: 10.1063/5.0146064
Submitted: 9 February 2023 • Accepted: 30 July 2023 •
Published Online: 16 August 2023

Rene Celis-Cordova, Jacob J. Gose,[a] Abigail F. Brown, AnnahMarie G. Behn, Matthew Huebner, Ethan M. Williams, Yang Xiang, Jonathan D. Chisum, Alexei O. Orlov, and Gregory L. Snider

AFFILIATIONS

Department of Electrical Engineering, 275 Fitzpatrick Hall of Engineering, University of Notre Dame, Notre Dame, Indiana 46556, USA

[a]Author to whom correspondence should be addressed: jgose@nd.edu

ABSTRACT

A radio frequency (RF) reflectometry technique is presented to measure device capacitances using a probe station. This technique is used to characterize micro-electromechanical system (MEMS) variable capacitor devices that can be connected to create pull-up and pull-down networks used in digital gates for reversible computing. Adiabatic reversible computing is a promising approach to energy-efficient computing that can dramatically reduce heat dissipation by switching circuits at speeds below their RC time constants, introducing a trade-off between energy and speed. The variable capacitors in this study will be measured using single port RF reflectometry achieved with a custom-made RF probe. The RF probe consists of a micromanipulator with an on-board matching network and is calibrated by measuring a capacitive bank that shows a clearly visible frequency shift with the increase in capacitance. The RF probe worked well when measuring static capacitors with no parasitic resistance; however, the frequency shift is masked when measuring the MEMS variable capacitors due to their high in-series parasitic resistance (around 80 kΩ). Therefore, RF reflectometry has the potential to measure MEMS variable capacitors in the range of 0–30 fF when not masked by a high in-series parasitic resistance, creating a fast and versatile method for characterizing variable capacitors that can be used in energy-efficient computing.

I. INTRODUCTION

Adiabatic reversible computing is a promising approach to energy-efficient computing that can dramatically reduce heat dissipation by switching circuits slowly relative to their RC time constants, introducing a trade-off between energy and speed. CMOS circuits have been used to implement reversible computing[1,2] but are ultimately limited by leakage since the transistors do not turn completely off.[3] Micro-electromechanical system (MEMS) variable capacitors have been around for a few decades[4] and have applications in fields such as computing, chemical processes, biology, and medical applications. MEMS relays have been explored as alternative devices to eliminate leakage but are limited by the degradation of current-carrying contacts.[5] We are investigating a novel MEMS device based on a coupled variable capacitive network that will be a key element for reversible adiabatic logic (ACL).[6] In ACL, variable capacitors implement pull-up and pull-down networks to create electrostatically coupled digital gates.[7] Since the capacitors do not need make-and-break electrical contacts, they neither suffer from the degradation of contacts[8] nor pass any DC currents. As a result, Joule heating is minimized, leading to extremely low static power dissipation.[6] Since the operation of the device depends on the change of capacitance in small structures rather than the change of resistance when a transistor turns on and off or when a nanorelay closes, a new approach is needed to characterize the devices.

A diagram of the voltage-controlled variable capacitor is presented in Fig. 1. The gap closing structure resembles a relay but contains an insulator in the cantilever to create two separate capacitors: C_{in} and C_S. The cantilever is controlled by the input capacitor C_{in}, which is electrically isolated from the output series connection of capacitors C_S and C_0. When a voltage V_{in} is applied to the input, the cantilever moves down, increasing C_S and, thus, increasing the voltage V_{out}. When the voltage is removed, the cantilever moves back up, restoring the capacitors C_{in} and C_S to their original values and,

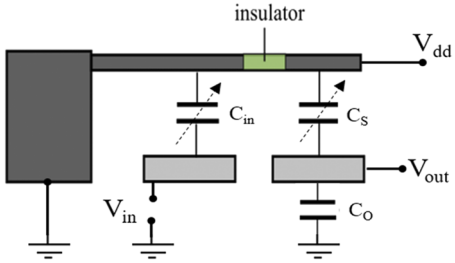

FIG. 1. MEMS device for adiabatic capacitive logic.

thus, lowering the voltage V_{out}. With a careful choice of capacitance values and voltages, energy level restoration can be achieved in ACL logic.

The devices are fabricated on silicon wafers using surface micromachining techniques. A top view of the basic variable capacitor device is presented in Fig. 2(a), with a cross-section in Fig. 2(b). The suspended cantilever is connected to polysilicon springs that will allow the cantilever to move down. The springs are anchored to the substrate and connected to bottom TiN wires that carry the electrical signals in and out of the device.

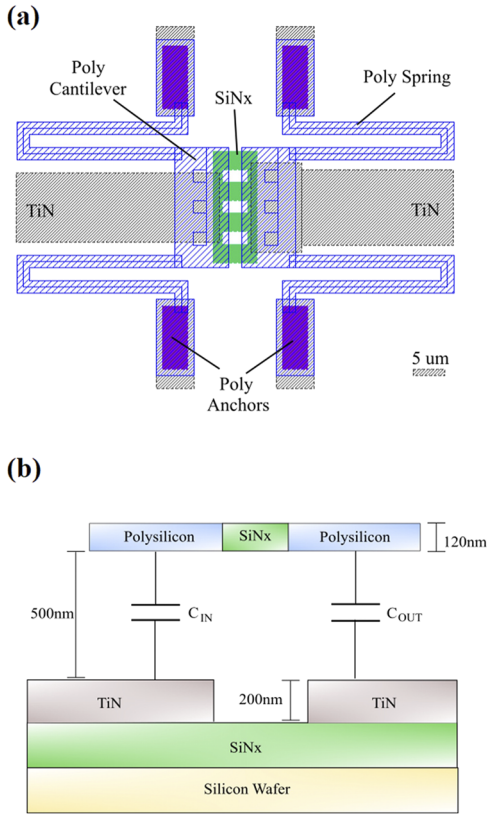

FIG. 2. (a) Top view of MEMS variable capacitors. (b) Cross-section diagram.

II. DEVICE CHARACTERIZATION

Characterizing the operation of these MEMS devices is a challenge since the small size of the structure results in a small capacitance value. Accurate measurements of the change in capacitance would typically require wire bonding and packaging of the device, a time-consuming process. The method presented here uses single port radio frequency (RF) reflectometry, which measures the change in the resonant frequency of a matching network due to a change in capacitance. The matching network is integrated into an analytical probe and probe station, forming a very versatile measurement system.

A. RF probe

The MEMS ACL variable capacitor device can be viewed as a four terminal variable capacitance device, as shown in Fig. 3(a), where the change of the input capacitance C_{IN} driven by gate voltage Vg results in the change of the mechanically coupled output capacitance C_{OUT}.

A simple way to measure C_{OUT} is to include it in the resonant matching network[9] (MN) assembled as part of the RF probe. A simplified diagram of the reflectometry setup is presented in Fig. 3(b). It shows the RF signal passing through a directional coupler that splits the forward and reflected signals. The forward signal RF_{IN} is applied to the MN, which includes C_{OUT}. The reflected signal, RF_{OUT}, is amplified using a low noise preamplifier attached to the coupler. RF signal generation and rectification are performed by a UHF Zurich Instruments lock-in amplifier,[10] and the changes in the phase and magnitude of the reflection coefficient due to the change in the capacitor are recorded.

The purpose of MN is to convert the frequency dependent impedance of the load, Z(f), in our case the output capacitor of the ACL device, to an impedance close to that of the line $Z_0 = 50\ \Omega$. In this case, at a resonant frequency $f = f_R$, the magnitude of the reflection coefficient,

$$\Gamma = \frac{Z_{Load}(f) - Z_0}{Z_{Load}(f) + Z_0} \tag{1}$$

is minimized. The value of C_{OUT} for the circuit in Fig. 1(b) defines the resonant frequency of MN. The MN used in our experiments is composed of a 20 mm long section of transmission line (TL) (coax cable, 0.047 in. in diameter, with a sharpened end of the central conductor that enables good contact with a bonding pad of output capacitance of the ACL device, C_{OUT}, or a pad of a test capacitor in the calibration capacitance bank); a surface mount 68 nH inductor (0805CS by Coilcraft)[11] in series with TL; and a balancing capacitor C_{bal} to ground that enables tuning of the MN to achieve close to matching conditions. The other end of the measured capacitor is connected to the ground of the RF probe using an analytical probe tip also connected to the ground of the RF probe.

A calibration/error correction (CEC) protocol using Short, Open, and Load standards is applied to remove non-idealities of the setup down to the reference plane [shown by a dashed red line in Fig. 3(a)], as described in Ref. 12. To calibrate the probe, we used an array of size 0603 capacitors by Johansson (0.3, 0.5, 0.8, 1.0 1.2, and 1.5 pF) with one end of each vertically-oriented capacitor soldered to a copper plate, while the other end is exposed and can be contacted

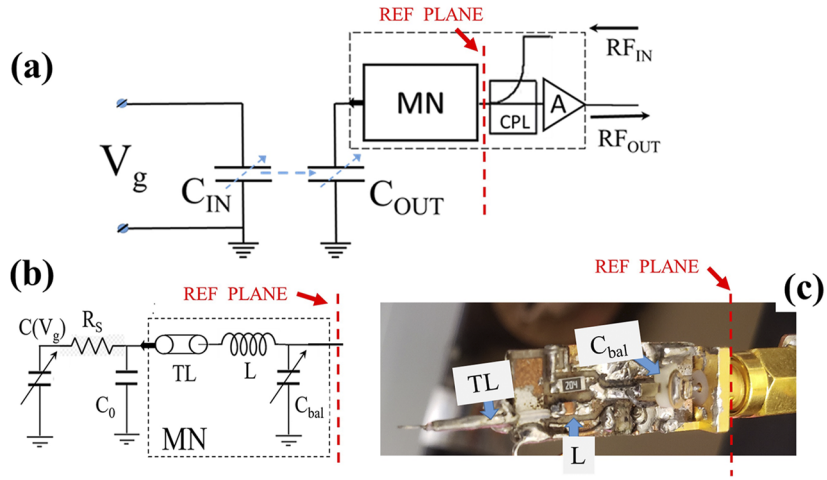

FIG. 3. (a) Simplified circuit diagram of the measurement of the ACL device. The components in the dashed line box represent the RF probe. MN is a matching network, A is a preamplifier (Minicircuits ZX60 -P103LN+), and CPL is a directional coupler (ZX30-17-5-S+). (b) Matching network circuit diagram, and (c) photo of the probe. The Reference plane is shown by the dashed red line. Components of a matching network: TL-a piece of transmission line, 19.5 mm long, L = 68 nH inductor, C_{bal} = Trimmer 1–11 pF, R_S is the series resistor of the ACL device, and $C(V_g)$ is the ACL output capacitor.

by the RF probe. The copper plate is connected to the ground of the RF probe by a copper braid.

Since the expected value of the varying part of C_{OUT} for ACL devices, $C_{ACL} = \Delta C_{OUT}$, is on the order of 0.03 pF, the MN is tuned to achieve matching conditions for the probe above the surface of the sample ("air" curve in Fig. 4). Experimental results with the capacitor array show a clearly visible frequency shift with the increase in capacitance C_{cal}. We perform SPICE simulations of the probe with variable capacitance using the Advanced System Design (ADS) software from Keysight, as shown in Fig. 5(a).[13] Here, the simulation includes the required capacitors, the circuit model for the inductor, and the model for the coaxial cable.

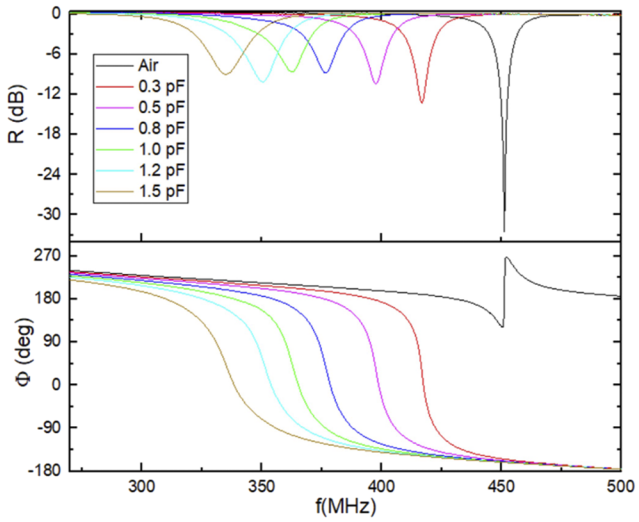

FIG. 4. Error–corrected experimental results showing the shift of resonant frequency along with the change of matching conditions when the RF probe is in contact with capacitors in the capacitor bank. The balancing capacitor is tuned to achieve close to matching conditions for the probe lifted up in the air (C_{bal} = 11.5 pF).

The realistic inductor SPICE model corresponds to the lumped element model for a Coilcraft 68 nH inductor (0805CS) that includes its parallel capacitance and skin effect resistance. The coaxial tip is modeled as a transmission line with the corresponding loss (14 dB/m) and length (18.5 mm). The parasitic capacitances on each side of the coaxial cable are set at 0.001 pF. We varied the values of the capacitor C_{ACL} to obtain the same resonant frequency as in the experiment. The results shown in Figs. 5(b) and 5(c) demonstrate a reasonably strong correlation with the experimental data. The systematic difference between the measured and simulated values in Fig. 5(b) is likely attributed to unaccounted parasites. Generally, equivalent circuits are valid within a specific frequency range centered around the operating frequency, and given the extremely wide frequency range of variation, we found this agreement to be quite satisfactory. Considering that the operation of the ACL device typically involves much smaller changes in capacitance we are confident in our model's ability to accurately detect small variations in capacitance, with a high level of precision.

Next, we perform a simulation to mimic the expected action of the ACL device and trace a capacitance variation in the range 0–30 fF either by measuring the changes in amplitude and phase of the reflection coefficient [Fig. 5(c)] or by tracking the resonant frequency of the network using a phase locked loop (option available on UHFZI clock-in).

These results show that the RF reflectometry system has the potential to measure MEMS variable capacitors in the range of interest (0–30 fF). This would represent a direct measurement of the change in capacitance in MEMS ACL variable capacitors and would pave the way for their use in adiabatic reversible computing.

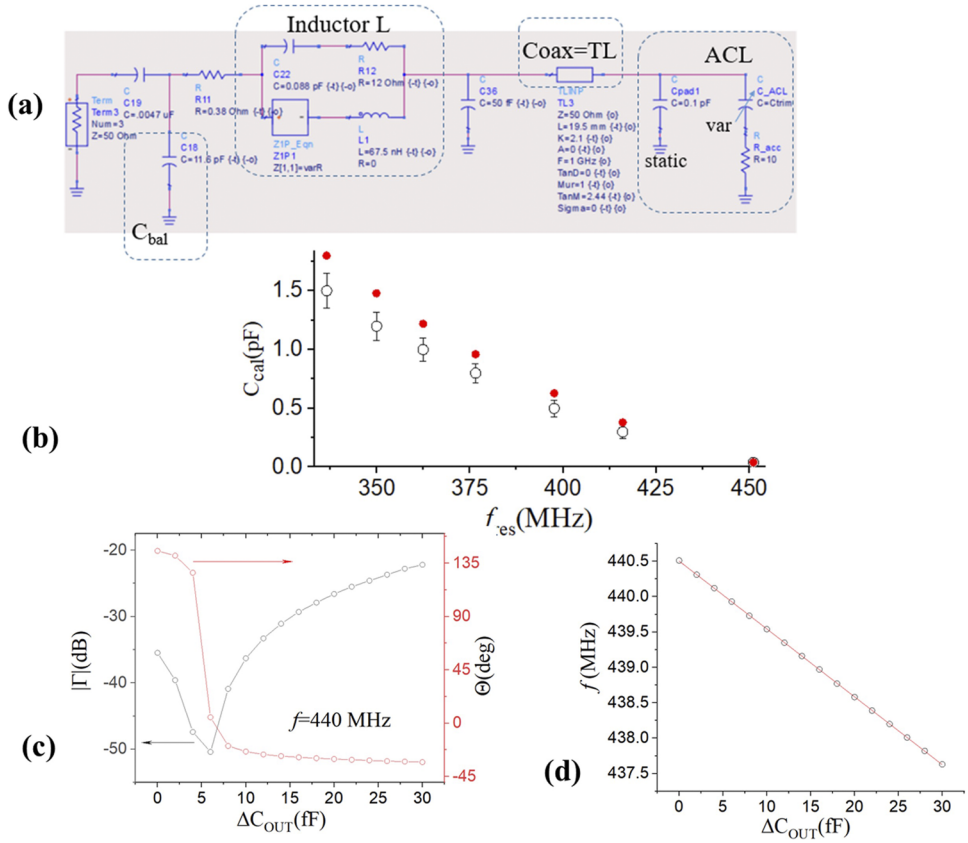

FIG. 5. (a) Simulated circuit for testing the ACL. The output capacitor is simulated as a parallel combination of the static pad capacitor C_{pad} = 0.1 pF and the variable capacitor $C_{ACL} = \Delta C_{OUT}$ in series with the ACL beam resistor R_{acc}. Note that variations of R_{acc} in the range 0–100 Ω have little impact on the results, leading to a small variation of magnitude $\Gamma < 0.5$ dB for all ΔC_{OUT} in the range and no shift in resonant frequency. (b) Comparison to a capacitor array. Simulated (red dots) C_{OUT} was needed to obtain the experimentally observed resonant frequencies, along with measured values of C_{OUT} (black dots). The capacitance of the probe in "Air" is assumed to be 0.04 pF. (c) Simulated $|\Gamma|$ and Θ for ΔC_{OUT} changing in the range 0–30 fF; the probe signal frequency is set to 440 MHz. (d) Frequency shift vs ACL ΔC_{OUT}.

B. Variable capacitance measurement

After the reflectometry system is verified using static capacitors, the MEMS gap-closing devices are connected to the RF reflectometry system following the diagram presented in Fig. 6. Here, the parasitic capacitance that arises from the wires and pads of the integrated circuit containing the MEMS devices is 0.1 pF. The parasitic resistance of the TiN wires is also included in the model since their resistance of around 80 kΩ represents a considerable impedance in the system. The reflectometry system connected to ACL MEMS capacitors should be able to detect the change in capacitance as a gate voltage is applied and the variable capacitors increase from 2.8 to 35.2 fF, according to the physical simulation results of the MEMS devices.[14]

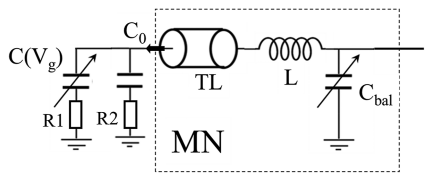

FIG. 6. RF reflectometry system that includes the capacitors of the MEMS devices under test with their series parasitic resistance arising from the titanium nitride wires.

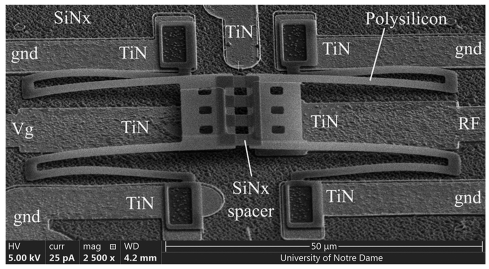

FIG. 7. SEM micrograph of MEMS ACL devices for RF reflectometry showing the required connections.

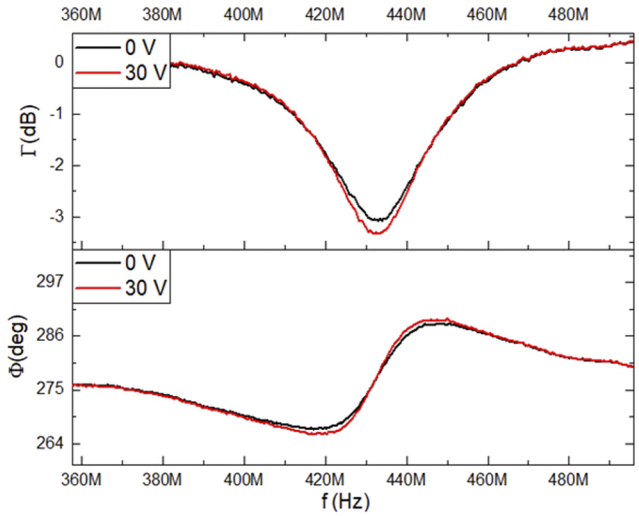

FIG. 8. Reflected signal magnitude and phase of ACL MEMS devices with a gate bias of 0 and 30 V.

An SEM micrograph with the corresponding RF connections labeled on the device is presented in Fig. 7. The polysilicon cantilever is grounded on both sides, since the left side of the cantilever is used as the actuator to move down the mechanical structures, and the right side of the cantilever corresponds to the variable output capacitor meant for adiabatic reversible computing. The left TiN electrode under the cantilever is connected to the gate voltage V_g, while the right TiN electrode under the cantilever is connected to the RF micromanipulator probe for reflectometry measurements. The rest of the interconnections leading to bonding pads are not shown in the SEM micrograph but are included as parasitic capacitance and resistance in the reflectometry model to better represent the results obtained.

The magnitude and phase of the reflected coefficient for MEMS gap-closing capacitors at two different gate voltages are presented in Fig. 8. When there is no gate bias applied to the MEMS device, the cantilever does not move and stays in the up position. When a bias is applied to the gate, the cantilever moves down, increasing the capacitance of the device until it reaches the pull-in voltage, and the cantilever stays down. The motion of the cantilever can be seen under an optical microscope.

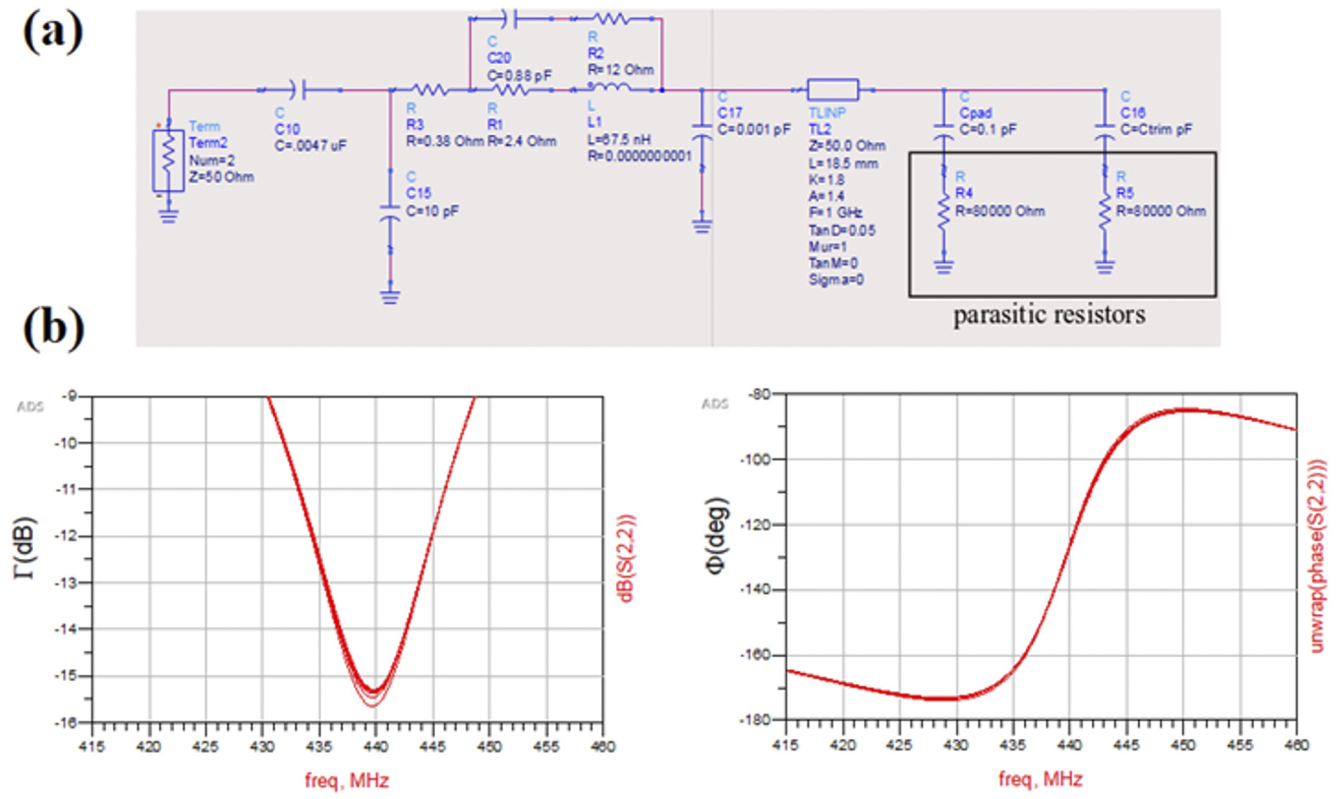

FIG. 9. (a) Reflectometry system simulation circuit, including the parasitic resistance of the device under test. (b) Simulation results of the reflection coefficient for a variable capacitor ranging from 2.8 to 35.2 fF in steps of 5 fF.

Unfortunately, the change in the MEMS variable capacitance could not be reliably measured using the setup described above. Here, both the phase and the magnitude of the reflection coefficient show very little change. Furthermore, the resonant frequency does not change between the two configurations presented.

As shown in Fig. 8, the change in capacitance does not produce a change in the resonant frequency of the reflectometry system. This is due to the parasitic resistance of the MEMS devices that arises from the titanium nitride layer used as described above. The impedance of the 80 kΩ resistor has an undesirable effect on the parasitic resistance of the TiN wires since the vapor HF etches some of the titanium nitrides during the release process, therefore increasing the resistance of the wires. Future generations of ACL devices would benefit from reducing the resistance of the wires by coating the TiN with a metal, such as gold, that prevents etching when exposed to vapor HF.

The SPICE ADS simulation of the RF reflectometry system measuring a variable capacitor with an 80 kΩ parasitic resistance in series confirms the behavior observed during the experiment described above. The simulation presented in Fig. 9 shows that an increase in capacitance does not change the resonant frequency. Even though the RF probe works well with samples that have negligible parasitic resistance, the considerable resistance in the wires of ACL devices makes reflectometry an unsuitable measurement technique for their variable capacitance since the impedance of the resistors is higher than the capacitors at RF frequencies. At a frequency of 430 MHz, the impedance of a 35 fF capacitor is only 10.5 kΩ, and this is masked by the 80 kΩ parasitic resistance.

III. FUTURE WORK

We are in the process of developing the next generation of ACL MEMS devices where parasitic capacitance and resistance are drastically reduced.[15] The reduction in parasitic capacitance is accomplished by fabricating the MEMS ACL devices on an insulating (fused silica) substrate instead of a semiconducting (silicon) substrate. Moreover, the use of a thicker insulating substrate reduces the parasitic capacitance from the interconnections and bonding pads when compared to those on a silicon substrate. Experiments show that the value of C_{pad} drops by a factor of >4. The reduction in the parasitic resistance in the wires down to the desired range of 10–100 Ω that ensures predicted behavior in the 100+ MHz range of operation can be accomplished by depositing Au on top of the titanium nitride wires. The TiN layer is still needed to grow the polysilicon anchors using low-pressure chemical vapor deposition. MEMS using gold have been demonstrated to withstand the release process[16] and could dramatically lessen resistance. Furthermore, the resistance of the polysilicon, cantilever can be reduced by using a platinum silicide process.[17] Here, platinum is evaporated on top of the polysilicon and a platinum silicide is formed by rapid thermal annealing. The cross-section diagram of the proposed ACL MEMS devices is presented in Fig. 10.

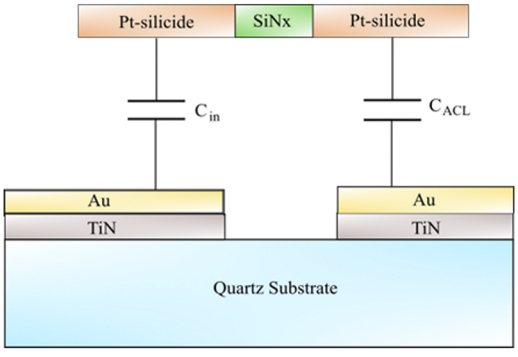

FIG. 10. ACL cross-section with quartz substrate and reduced resistance.

IV. CONCLUSION

We demonstrate a versatile RF probe measurement system meant for reflectometry measurements of variable capacitance. The RF probe has the capability of measuring the capacitance change in MEMS variable capacitors that have negligible in-series resistance. However, the measurement of variable output capacitance in its current implementation of MEMS ACL is hampered by several parasitic components, namely, a large (~100 kΩ) in-series resistance of the access wires and voltage- and illumination-dependent parallel capacitance from the substrate that masks the reflectometry measurements, despite being visible in the microscope motion of the ACL body. Modifications for next-generation ACL devices are proposed, which use an insulating substrate and gold as a conductor to reduce parasitic capacitance and resistance, respectively.

ACKNOWLEDGMENTS

This work was supported by the National Science Foundation. (Grant No. ECCS-1914061).

This work was performed in part at the Cornell NanoScale Facility, a member of the National Nanotechnology Coordinated Infrastructure (NNCI), which is supported by the National Science Foundation (Grant No. NNCI-2025233). The authors are thankful to Anirban Chowdhury for reading the manuscript and making useful suggestions.

AUTHOR DECLARATIONS

Conflict of Interest

The authors have no conflicts to disclose.

Author Contributions

Rene Celis-Cordova: Conceptualization (lead); Formal analysis (lead); Investigation (lead); Methodology (lead); Project administration (lead); Writing – original draft (lead); Writing – review & editing (equal). **Jacob J. Gose**: Formal analysis (equal); Investigation (equal); Writing – review & editing (equal). **Abigail F. Brown**: Formal analysis (equal); Investigation (equal); Writing – review & editing (equal). **AnnahMarie G. Behn**: Formal analysis (equal); Investigation (equal); Writing – review & editing (equal). **Matthew Huebner**: Data curation (equal); Investigation (equal); Validation (equal). **Ethan M. Williams**: Investigation (equal). **Yang Xiang**: Formal analysis (equal). **Jonathan D. Chisum**: Software

(equal); Supervision (equal). **Alexei O. Orlov**: Investigation (equal); Software (equal); Supervision (equal); Writing – review & editing (equal). **Gregory L. Snider**: Investigation (equal); Supervision (equal); Writing – review & editing (equal).

DATA AVAILABILITY

The data that support the findings of this study are available from the corresponding author upon reasonable request.

REFERENCES

[1]S. G. Younis and T. F. Knight, *Research on Integrated Systems* (MIT Press, Cambridge, MA, 1993), pp. 234–250.
[2]R. Celis-Cordova, A. O. Orlov, T. Lu, J. M. Kulick, and G. L. Snider, in *Proceedings of the 2019 Fourth IEEE International Conference on Rebooting Computing (ICRC)* (IEEE, 2019), pp. 106–109.
[3]K. J. Kuhn, IEEE Trans. Electron Devices **59**(7), 1813–1828 (2012).
[4]K. E. Petersen, IBM J. Res. Dev. **23**(4), 376–385 (1979).
[5]S. Rana, J. Mouro, S. J. Bleiker, J. D. Reynolds, H. M. H. Chong, F. Niklaus, and D. Pamunuwa, Nat. Commun. **11**(1), 1181 (2020).
[6]G. Pillonnet, H. Fanet, and S. Houri, in *2017 IEEE International Symposium on Circuits and Systems (ISCAS)* (IEEE, 2017), pp. 2767–2770.
[7]Y. Perrin, A. Galisultanov, L. Hutin, P. Basset, H. Fanet, and G. Pillonnet, IEEE Trans. Electron Devices **68**(6), 2938–2943 (2021).
[8]H. Samaali, Y. Perrin, A. Galisultanov, H. Fanet, G. Pillonnet, and P. Basset, Nano Energy **55**, 277–287 (2019).
[9]M. Thompson and J. K. Fidler, IEEE Trans. Circuits Syst. I **51**(10), 2098–2106 (2004).
[10]Zurich Instruments, https://docs.zhinst.com/uhf_user_manual/overview.html, 2023.
[11]Coilcraft, Inc. https://www.coilcraft.com/en-us/products/rf/ceramic-core-chip-inductors/0805-(2012)/0805cs/, 2012.
[12]M. J. Filmer, M. Huebner, T. A. Zirkle, X. Jehl, M. Sanquer, J. D. Chisum, A. O. Orlov, and G. L. Snider, Sci. Rep. **12**(1), 3098 (2022).
[13]T. T. Oo, A. D. M. Africa, and R. F. Navea, J. Phys.: Conf. Ser. **1997**(1), 012007 (2021).
[14]R. Celis-Cordova, A. O. Orlov, and G. L. Snider, in *2020 IEEE Silicon Nanoelectronics Workshop (SNW)* (IEEE, Honolulu, HI, USA, 2020), pp. 115–116.
[15]Y. Mafinejad, A. Z. Kouzani, and K. Mafinezhad, in *Tencon IEEE Region* (IEEE, Singapore, 2009), Vol. 10, p. 411.
[16]L. C. Ni and M. P. de Boer, J. Microelectromech. Syst. **30**(3), 426–432 (2021).
[17]E. Alptekin, M. C. Ozturk, and V. Misra, IEEE Electron Device Lett. **30**(4), 331–333 (2009).